Available online at www.sciencedirect.com
ScienceDirect
Optical Materials 31 (2008) 28–34
OPTICAL Materials
www.elsevier.com/locate/optmat

Study on mid-IR NLO crystals $CsGe(Br_xCl_{1-x})_3$

Zhi-Guang Lin [a,*], Li-Chuan Tang [b], Chang-Pin Chou [a]

[a] Department of Mechanical Engineering, National Chiao Tung University, Hsinchu 305, Taiwan, ROC
[b] Department of Electrical Engineering, Chung-Cheng Institute of Technology, National Defense University, Taoyuan 353, Taiwan, ROC

Received 25 July 2007; received in revised form 13 November 2007; accepted 1 January 2008
Available online 7 March 2008

Abstract

An innovative infrared nonlinear optical crystal $CsGe(Br_xCl_{1-x})_3$ was synthesized. From its powder X-ray diffraction pattern, this crystal was characterized as a rhombohedral structure with a (*R*3*m*, No. 160) space group symmetry. The powder second-harmonic generation (PSHG) measurement of $CsGeBr_3$ showed that its nonlinear optical efficiency is 9.64 times larger than that of rhombohedral $CsGeCl_3$ and is 28.29 times larger than that of KH_2PO_4 (KDP), and most important of all, that $CsGe(Br_xCl_{1-x})_3$ is phase-matchable. The infrared transparent spectrum of rhombohedral $CsGe(Br_xCl_{1-x})_3$ was extended to more than 30 μm. The rhombohedral $CsGe(Br_xCl_{1-x})_3$ shows the potential in the realm of nonlinear optics and can be applied to the infrared region.

PACS: 61.50.Nw; 61.66.Fn

Keywords: Solid solutions; Halides; Nonlinear optic materials; Noncentrosymmetric; Second-harmonic generation

1. Introduction

Second-order nonlinear optical (NLO) materials played a key role in such optical fields as laser frequency conversion and optical parametric oscillation/amplification OPO/OPA) [1,2]. For inorganic second-order NLO materials, several crystals used in ultraviolet (UV) and visible regions were proposed in the past two decades, such as KH_2PO_4 (KDP), $KTiOPO_4$ (KTP), β-BaB_2O_4 (BBO), LiB_3O_5(LBO). But in the infrared (IR) region the current materials, such as $AgGaSe_2$, $ZnGeP_2$, are not good enough for applications mainly due to their low laser damage threshold, as their bandgaps were smaller than 1.5 eV. So the search for new NLO crystals with excellent properties, especially a high damage threshold, has become one of the key research areas in NLO material science and laser technology [3].

Up to now, several ternary halides were discovered to exhibit second-order NLO properties, such as ABX_3 (A = Cs; B = Ge; X = Cl, Br, I) [4–6]. And CGC's damage threshold reaches 200 MW/cm^2 [7]. Ternary halides [4,5] recently became a new category of nonlinear optical materials, which were potentially applicable from visible to infrared spectrums. Owing to the optical damage threshold and the transparent range of materials related to the magnitude of the bandgap, while the optical non-linearity is inversely proportional to the cubic power of the band gap [8], the linear and NLO properties of $CsGe(Br_xCl_{1-x})_3$ can be adjusted by varying the alloy composition. In this paper, the synthetic method of crystals and measurements of the optical properties in each composition are reported. Nonlinear coefficients of $CsGe(Br_xCl_{1-x})_3$, $x = 0$, 1/6, 2/6, 3/6, 4/6, 5/6, 1 are also carried out to reveal the potential of these crystals in NLO applications.

2. Experimental

2.1. Synthesis

The procedure of synthesis was modified from the work done by Gu et al. [9,7,10]. Chritensen and Tananaev et al.

* Corresponding author. Tel.: +886 3 5712121 55157; fax: +886 3 5720634.
E-mail address: zglin.me91g@nctu.edu.tw (Z.-G. Lin).

0925-3467/$ - see front matter © 2008 Elsevier B.V. All rights reserved.
doi:10.1016/j.optmat.2008.01.004

[11,12] used different synthesis methods, but their methods seemed complex and the productivity was poor. In this study, H_3PO_2 (50%) was loaded with HBr (48%), HCl (37%), and GeO_2 (99.999%) into a 250 ml beaker, and then heated to 95 °C. The solution was vigorously mixed for 5 h and then cooled to room temperature. After removing the precipitate, CsCl (99.9%) was added and the temperature was raised to boiling. Then the mixture was naturally cooled to room temperature again. A light yellow precipitate was formed. The reaction equations were listed as follows:

$$H_3PO_2 + 6xHBr + 6(1-x)HCl + 2GeO_2 = H_3PO_4 + 2HGe(Br_xCl_{1-x})_3 + 2H_2O$$

then

$$HGe(Br_xCl_{1-x})_3 + CsCl = CsGe(Br_xCl_{1-x})_3 \downarrow + HCl$$

Recrystallization was done by mixing the precipitate with 1:1 concentrated HX and alcohol solution to give the yellow crystals $CsGe(Br_xCl_{1-x})_3$. To avoid the residue of precursor, we repeat this procedure by seven times. Then, the crystals were dried at 85 °C for 48 h under vacuum to prevent the influence of the deliquescence. The color of precipitated product varied from yellow to white as soon as the substitutional ratio, x, changed from 1 to 0.

2.2. Physical measurements

$CsGe(Br_xCl_{1-x})_3$ crystal was synthesized and sieved into different particle sizes in order to measure and analyze its structural and optical properties. The crystal structures were observed using an X-ray diffractometer. The composition of all samples was measured by electron-probe X-ray microanalysis (EPMA). The optical transmission spectra in the infrared region was determined by a Fourier-transform infrared spectrometer (FTIR) while the absorption edge was measured by UV–visible spectrometer. Linear optical properties were measured by an ellipsometer. Nonlinear optical properties were determined by powder second-harmonic generation measurements.

3. Results and discussion

3.1. Composition and structural properties

The results of Table 1 reveal that those samples possess a Cs to Ge ratio of almost 1:1. Besides, EPMA measurement can qualitatively confirm that bromine atoms were successfully doped in $CsGeCl_3$ crystal. There are still some impurities contained, but they are all smaller than 1% ($O_{max} \leqslant 0.52\%$, $P_{max} \leqslant 0.61\%$).

X-ray diffraction (XRD) measurement was employed to determine the structural parameters of all the crystals $CsGe(Br_xCl_{1-x})_3$. The synthesized crystals were crushed, ground, and sieved. X-ray diffractograms were obtained at room temperature by means of Cu Kα radiation with Siemens D5000 equipment. For determination of the lattice parameters, an extra CsCl crystal was used as an internal standard. The measured pattern was indexed and analyzed, i.e. the full-profile Rieltvelt refinement, by a non-profited program PowderCell [13], which was developed by W Kraus and G Nolze. The structural parameters of $CsGe(Br_xCl_{1-x})_3$ were compared with both $CsGeCl_3$ and $CsGeBr_3$, which were reported in JCPDS [14–18]. The peak-splitting phenomenon arised from the rhombohedral distortion of the pseudo-cubic unit cell, mainly occurs from $2\theta = 15°$ to 35° (see Fig. 1). And the X-ray diffraction peaks shifted gradually according to the substitute composition. There were certain stronger diffraction peaks observed at $2\theta = 31.76°$, 27.66°, 26.86°, 22.60°, 22.10°, 15.76° in $CsGeBr_3$. These diffraction patterns were compared with JCPDS and were indexed with (200), $(1\bar{1}1)$, (111), $(1\bar{1}0)$, (110) and (100) planes, respectively. The splitting differences between $(1\bar{1}1)$ with (111) and $(1\bar{1}0)$ with (110) are getting closer as the containment of Br is decreasing in $CsGe(Br_x\ Cl_{1-x})_3$. Table 2 lists the observed d values compared with those in the literature.

In an ideal perovskite structure, the cell parameters were $a = b = c$ and $\alpha = \beta = \gamma = 90°$ with cubic space group

Table 1
The composition (at.%) of the rhombohedral NLO crystals $CsGe(Br_xCl_{1-x})_3$ ($x = 0$, 1/6, 2/6, 3/6, 4/6, 5/6, 1) from EPMA measurements

	$x = 0/6$	$x = 1/6$	$x = 2/6$	$x = 3/6$	$x = 4/6$	$x = 5/6$	$x = 6/6$
Cs	20.56	20.14	20.18	20.57	20.42	20.42	20.32
Ge	20.66	20.22	20.34	20.61	20.27	20.31	20.51
Br	0	10.31	20.38	30.15	40.01	48.06	58.17
Cl	58.04	48.57	37.97	27.74	18.60	10.10	0
O	0.45	0.45	0.52	0.35	0.34	0.50	0.46
P	0.29	0.31	0.61	0.58	0.36	0.61	0.54

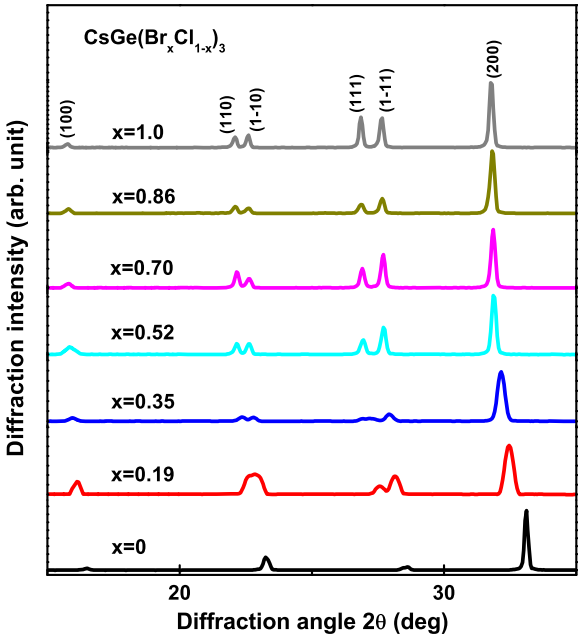

Fig. 1. The X-ray powder diffraction results for nonlinear optical crystals $CsGe(Br_x\ Cl_{1-x})_3$. It can be seen that the XRD peaks shift with Br composition.

Table 2
Diffraction data of $CsGe(Br_x\ Cl_{1-x})_3$ crystals

$CsGe(Br_x\ Cl_{1-x})_3$		$x = 0$		$x = 0.19$	$x = 0.35$	$x = 0.52$	$= 0.70$	$x = 0.86$	$x = 1$
(*hkl*)	*d* (lit.)/Å [4]	*d* (lit.)/Å [11]	*d* (obs.)/Å	*d* (obs.)/Å	*d* (obs.)/Å	*d* (obs.)/Å	*d* (obs.)/Å	*d* (obs.)/Å	*d* (obs.)/Å
(1 0 0)	5.466	5.484	5.372	5.498	5.560	5.602	5.602	5.609	5.623
(1 1 0)	3.863	3.862	3.825	3.925	3.977	4.013	4.013	4.022	4.022
(1 −1 0)	3.830	3.840	–	3.891	3.900	3.925	3.925	3.934	3.934
(1 1 1)	3.151	3.161	3.136	3.237	3.284	3.307	3.313	3.320	3.320
(1 −1 1)	3.129	3.134	3.120	3.169	3.197	3.220	3.220	3.225	3.225
(2 0 0)	2.712	2.721	2.705	2.758	2.783	2.809	2.809	2.813	2.817
(2 1 1)	2.231	2.230	2.224	2.283	2.314	2.334	2.337	2.340	2.343
(2 −1 1)	2.215	2.218	2.213	2.245	2.261	2.278	2.279	2.282	2.286
(2 2 0)	1.928	1.930	1.923	1.968	1.992	2.009	2.009	2.013	2.016
(2 −2 0)	1.920	1.919	1.913	1.938	1.954	1.966	1.968	1.970	1.972
(3 1 0)	1.723	1.725	1.719	1.775	1.775	1.788	1.790	1.793	1.795
(3 −1 0)	1.717	1.717	1.715	1.747	1.751	1.767	1.767	1.770	1.772
(3 1 1)	1.646	1.647	1.642	1.683	1.704	1.718	1.719	1.722	1.725
(3 −1 1)	1.638	1.640	1.637	1.663	1.680	1.691	1.693	1.696	1.697
(2 −2 2)	1.569	1.568	1.566	1.588	1.601	1.612	1.613	1.615	1.617
(4 0 0)	1.360	1.362	1.359	1.382	1.395	1.406	1.407	1.409	1.411

Pm-3m (No. 221). Examples are the higher temperature phase of cubic $CsGeCl_3$ ($a = b = c = 5.470$ Å, $\alpha = \beta = \gamma = 90°$ and $CsGeBr_3$($a = b = c = 5.362$ Å, $\alpha = \beta = \gamma = 90°$ [11,14–18]. From Table 3, the cell edges of rhombohedral (room temperature phase) $CsGeBr_3$ were longer than those of cubic (higher temperature) phase, and the cell angles of rhombohedral (room temperature phase) $CsGeBr_3$ became slightly smaller than 90°, which confirmed that $CsGeBr_3$ crystallized in the noncentrosymmetric rhombohedral phase. Structure parameters showed that the lattice constant became larger as Br increased while the cell angle became smaller as Br increased. Therefore, the structural distortion of $CsGe(Br_xCl_{1-x})_3$ will increase as Br increases. The structural distortion was one of the contributions of optical non-linearity. With perovskite-type ternary oxides ABO_3 as well as halides ABX_3, Goldschmidt's tolerance factor t_G [24,25] serves as a discriminating parameter of classifying perovskites in terms of structure modifications. The type of stacking depends on the tolerance factor t_G

$$t_G = \frac{(r_A + r_X)}{\sqrt{2}(r_B + r_X)}$$

where A is a large cation, B a smaller one, X is the anion and the *r* are the ionic radii of Shannon and Prewitt [26,27], which depend on the coordination number and bonding specimens. The tolerance factors, t_G, of $CsGeBr_3$ and $CsGeCl_3$ crystal structure are 1.009(4) and 1.027(2), respectively. They are close to the empirically ideal perovskite structure with $t_G = 1.0$. However, these values slightly deviate from the ideal value of perovskite structure, 1.0, and could be the reason for the structural distortion.

3.2. Linear optical properties

In Fig. 2, the absorption spectra measured at room temperature using $CsGe(Br_xCl_{1-x3}$ ($x = 0$, 1/6, 2/6, 3/6, 4/6, 5/6, 1) crystals in the UV–visible light range are shown. For the bandgap measurements, thin plates (≈500 μm) of $CsGe(Br_xCl_{1-x})_3$ were used. The recorded curves can be approximated with straight lines in the coordinates α^2 and $h\nu$, where α is the absorption coefficient and $h\nu$ is the photon energy. The straight line approximation is applied to the rapidly increasing portions of the curves in Fig. 2. Thus, the fundamental absorption edge is described by the $\alpha = A \cdot (h\nu - E_g)^{1/2}$ dependence, where A is a constant and the bandgap E_g can be determined from the cross points of the straight lines with the abscissa. This dependence corresponds to direct allowed electronic transitions [19]. In the inset of Fig. 2, the bandgap values are plotted versus Br composition. The absorption edge is found to decrease from 3.43 to 2.38 eV as the substitutional ratio, *x*, changed from 0 to 1.

Infrared spectra were recorded on the spectrometer (Bomem, DA8.3) in the range from 120 cm^{-1} to 4000 cm^{-1}, i.e. 2.5 μm to 83.3 μm, with the samples pressed into thin plates (≈500 μm). The transmittance of $CsGe(Br\text{-}_xCl_{1-x})_3$ plates were higher than 75% in the mid-infrared range. From Fig. 3, FTIR measurements showed that the long wavelength limit of the transparent range of the crystals exhibited a similar dependence on substitute composition. Crystal $CsGeCl_3$ had an infrared cut-off wavelength at approximately 30 μm, which was shorter than the cut-off value of $CsGeBr_3$ (approximately 47 μm). The infrared absorption edge of $CsGe(Br_xCl_{1-x})_3$ with $x = 1/6$, 2/6, 3/6, 4/6, 5/6 lay approximately from 32 to 38 μm. This result agreed with the effective-mass concept that the infrared transparency range of CGB is expected to be wider than that of CGC owing to the fact that the Br atom is heavier than Cl.

The results of the FTIR measurement at room temperature are presented in Fig. 4. The transmission range of the crystals extends wider as Br increases. The longest infrared transparency wavelength is usually limited by the phonon

Table 3
The refined unit-cell parameters of the diffraction patterns of $CsGe(Br_xCl_{1-x})_3$ crystals

$CsGe(Br_xCl_{1-x})_3$	a (=b = c) (Å)	α (= β = γ) (°)	Cell volume (Å^3)	t_G	Bond distances (Å) and angles (°)	
$x = 1$ (JCPDS)	5.635(9)	88.74(4)	178.6(5)	1.009(4)	Ge–Br 2.534(3)	Br–Ge–Br 95.16(9)
$x = 1$ (exp.)	5.637(5)	88.72(9)	179.0(4)		Ge–Br 3.116(4)	Br–Ge–Br 90.49(9)
						Br–Ge–Br 83.25(9)
$x = 0.86$ (exp.)	5.634(1)	88.72(9)	178.7(1)		Ge–Br 2.482(8)	Br–Ge–Br 96.28(8)
					Ge–Br 2.505(4)	Br–Ge–Br 96.28(4)
					Ge–Br 2.507(7)	Br–Ge–Br 96.19(4)
					Ge–Br 2.522(0)	Br–Ge–Br 95.56(0)
					Ge–Br 2.519(7)	Br–Ge–Cl 96.47(4)
					Ge–Cl 2.302(2)	Br–Ge–Cl 96.46(8)
$x = 0.70$ (exp.)	5.612(3)	88.74(5)	176.6(5)		Ge–Br 2.521(9)	Br–Ge–Br 95.77(4)
					Ge–Br 2.525(7)	Br–Ge–Br 95.35(1)
					Ge–Br 2.497(9)	Br–Ge–Cl 96.18(1)
					Ge–Br 2.439(9)	Br–Ge–Cl 96.14(3)
					Ge–Cl 2.290(2)	Cl–Ge–Cl 95.41(0)
					Ge–Cl 2.317(9)	
$x = 0.52$ (exp.)	5.590(0)	88.83(8)	174.5(7)		Ge–Br 2.526(3)	Br–Ge–Br 95.39(2)
					Ge–Br 2.526(3)	Br–Ge–Cl 96.34(8)
					Ge–Br 2.509(7)	Br–Ge–Cl 96.27(2)
					Ge–Cl 2.309(3)	Br–Ge–Cl 96.38(1)
					Ge–Cl 2.309(1)	Cl–Ge–Cl 95.48(2)
					Ge–Cl 2.306(5)	
$x = 0.35$ (exp.)	5.559(9)	89.01(8)	171.8(0)		Ge–Br 2.543(5)	Br–Ge–Br 95.13(4)
					Ge–Br 2.512(4)	Br–Ge–Cl 95.46(0)
					Ge–Cl 2.304(7)	Br–Ge–Cl 95.40(7)
					Ge–Cl 2.305(2)	Cl–Ge–Cl 96.04(8)
					Ge–Cl 2.330(0)	
					Ge–Cl 2.329(7)	
$x = 0.19$ (exp.)	5.478(7)	89.29(3)	164.4(1)		Ge–Br 2.529(6)	Br–Ge–Cl 95.43(5)
					Ge–Cl 2.312(3)	Cl–Ge–Cl 95.88(3)
					Ge–Cl 2.312(4)	Cl–Ge–Cl 95.37(4)
					Ge–Cl 2.321(8)	Cl–Ge–Cl 95.37(5)
					Ge–Cl 2.321(8)	Cl–Ge–Cl 95.52(2)
					Ge–Cl 2.337(9)	
$x = 0$ (exp.)	5.391(9)	89.70(5)	156.7(5)		Ge–Cl 2.348(2)	Cl–Ge–Cl 94.16(6)
$x = 0$ (JCPDS)	5.434(2)	89.72(3)	160.4(4)	1.027(2)	Ge–Cl 3.092(2)	Cl–Ge–Cl 89.66(5)
						Cl–Ge–Cl 86.23(5)

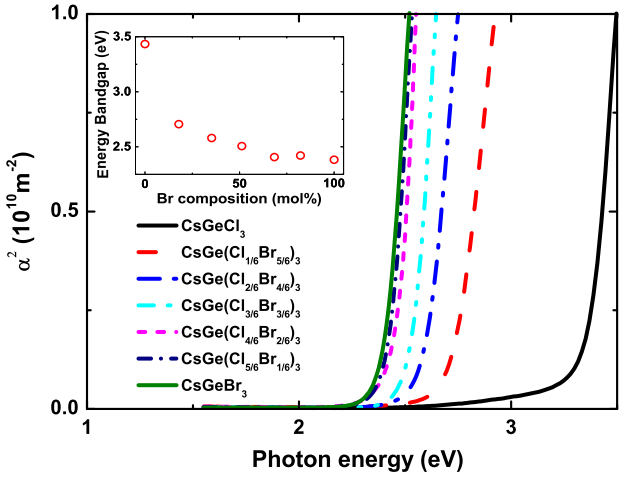

Fig. 2. Absorption coefficient near the band edge of $CsGe(Br_xCl_{1-x})_3$ plotted in coordinates α^2 and $h\nu$. The inset shows the Br composition dependence of E_g obtained.

absorption of the crystal. And the absorption edge is limited by the energy bandgap of the crystal.

Powder SHG measurements, which were reported by Chen et al. [20], were performed on a modified Kurtz-NLO [21] system using 1260 nm light. A mode-locked Cr^{4+}:Forsterite femtosecond laser with pulse duration 50fs, was used for all measurements. The Cr^{4+}:Forsterite oscillator gives pulses with a typical FWHM bandwidth of about 45 nm at a repetition rate of 76 MHz and average power of 270 mW. Since the SHG efficiency of powders has been shown to depend strongly on particle size [21,22], polycrystalline $CsGe(Br_xCl_{1-x})_3$ was ground and sieved (Newark Wire Cloth Company) into six distinct particle-size ranges, 19–37 μm, 37–74 μm, 74–105 μm, 105–210 μm, 210–420 μm and 420–840 μm (see Fig. 5). To make relevant comparison with known SHG materials, crystalline KDP was also ground and sieved into the same particle-size ranges. All of the powders were placed in separate capillary

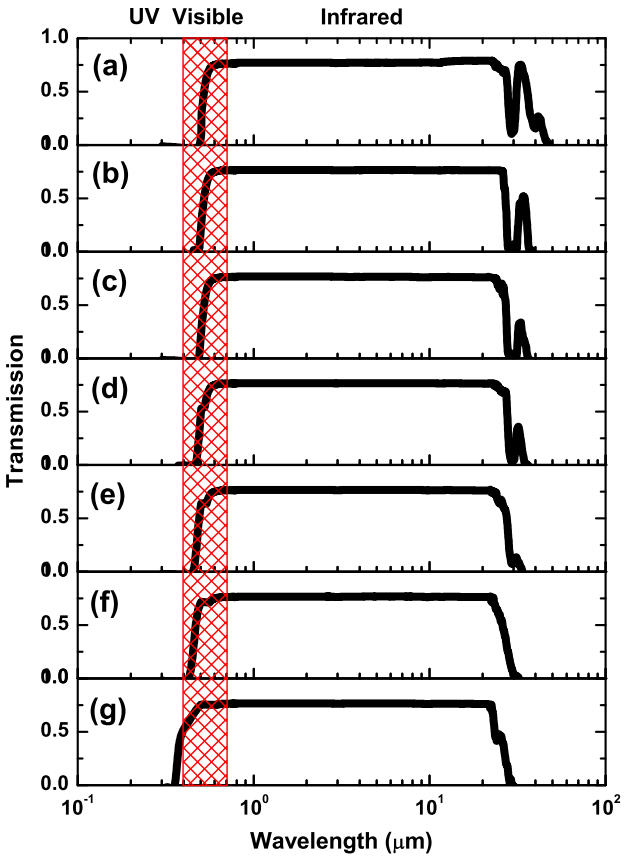

Fig. 3. The full transmission range of the nonlinear optical crystals $CsGe(Br_x Cl_{1-x})_3$: (a) $x = 1.00$; (b) $x = 0.86$; (c) $x = 0.70$; (d) $x = 0.52$; (e) $x = 0.35$; (f) $x = 0.19$; (g) $x = 0.00$.

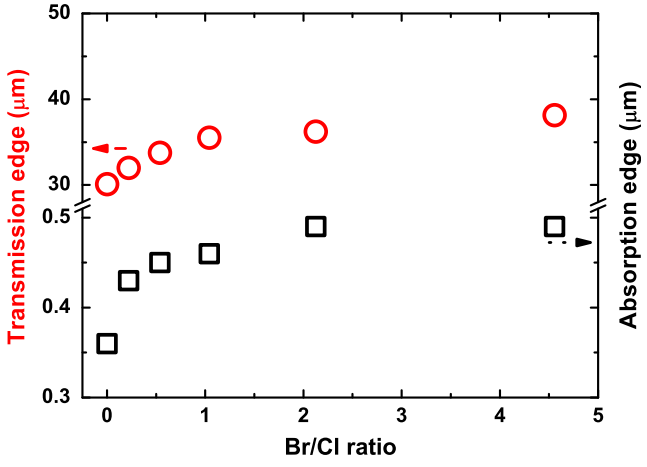

Fig. 4. The transmission edge and absorption edge of nonlinear optical crystals $CsGe(Br_xCl_{1-x})_3$.

tubes. The SHG radiation (630 nm) was collected in transmission and detected by a photomultiplier tube (Oriel Instruments). The SHG signal was collected by a data-acquisition (DAQ) interface and was monitored by a personal computer with the analysis program.

Powder SHG measurements on sieved polycrystalline $CsGe(Br_xCl_{1-x3}$ (Fig. 6) revealed that the SHG efficiencies

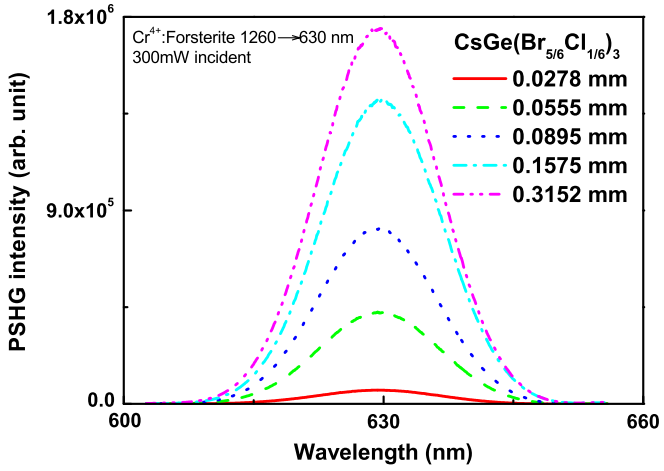

Fig. 5. The powder second-harmonic generation results for rhombohedral nonlinear optical crystals $CsGe(Br_{5/6}Cl_{1/6})_3$.

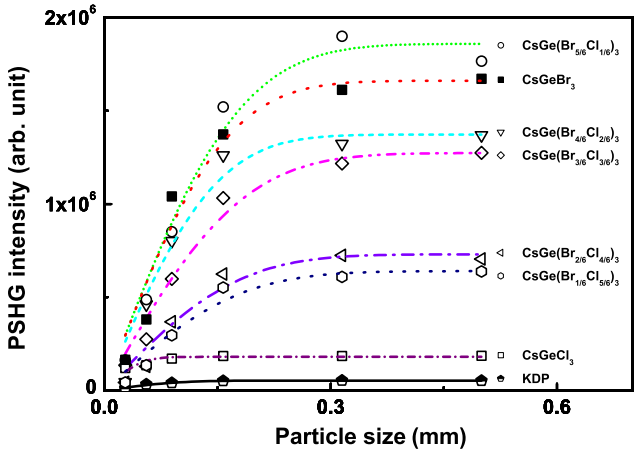

Fig. 6. The comparison of integrated powder second-harmonic generation intensity of nonlinear optical crystals KDP and $CsGe(Br_xCl_{1-x})_3$.

of $CsGe(Br_x Cl_{1-x})_3$ were higher than that of KDP. In addition, all of them were phase-matchable as was KDP, which meant that as the particle size became substantially larger than the coherence length of the crystal, the collected SHG intensity would not gain anymore and saturated at a certain value. The saturated PSHG intensities were estimated from the transmission signals in various particle sizes, and showed the SHG responses enhance as Br increases. Because the absorption coefficient of $CsGeBr_3$ in 630 nm was too large, the saturated PSHG intensity decayed. To modify such situation, the absorption coefficients (from Table 4) were adopted to calculate the real saturated PSHG intensity out. The d_{eff} values were calculated (by d_{KDP} (= 0.36 pm/V) [23]) and are shown in Fig. 7. The effective powder second-harmonic generation coefficients increased as Br increased. The non-linearity (see Fig. 8) of d_{eff}^2/n^3 of $CsGe(Br_x Cl_{1-x})_3$ crystals exhibited a similar dependence on substitution composition. There are some reasons for the significant SHG signals of rhombohedral $CsGe(Br_xCl_{1-x})_3$ crystals. First of all, the SHG responses were contributed from the structural distortion and the

Table 4
The ellipsometry measurements of the rhombohedral NLO crystals $CsGe(Br_xCl_{1-x})_3$

$CsGe(Br_x\ Cl_{1-x})_3$	$x = 0.00$	$x = 0.19$	$x = 0.35$	$x = 0.52$	$x = 0.70$	$x = 0.86$	$x = 1.00$
$\alpha_{630\ nm}$ (1/mm)	1.49	2.75	2.66	5.26	4.49	4.86	8.88
$n_{630\ nm}$	1.71	1.88	1.95	1.78	1.67	1.71	1.63

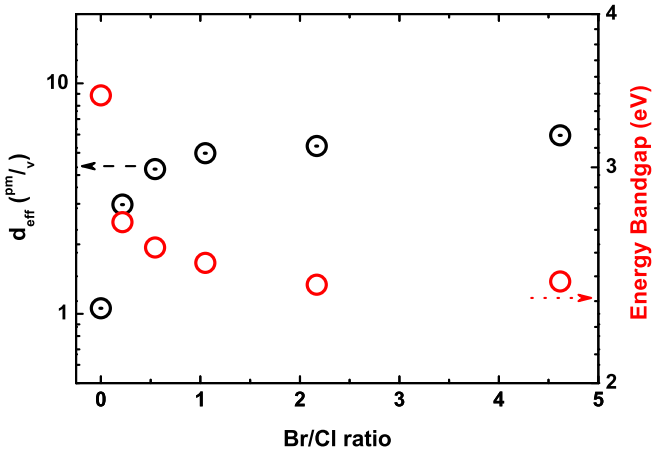

Fig. 7. The effective powder second-harmonic generation coefficients of nonlinear optical crystals $CsGe(Br_xCl_{1-x})_3$ and their energy bandgaps.

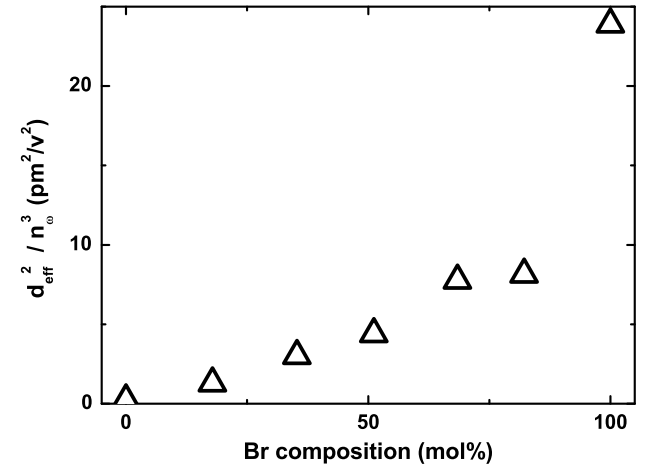

Fig. 8. The non-linearity of d_{eff}^2/n^3 for nonlinear optical crystals $CsGe(Br_xCl_{1-x})_3$.

off-centre Ge ion in the unit cell. From the results of XRD, the structural distortion increases as Br increases. And the cell angle distortion also becomes larger as Br increases. So the position of B-site cation, Ge, is closer to the cell corner as Br increases. Second, the optical non-linearity is approximately inversely proportional to the cube of the bandgap value [8]. So the bandgap values decreased and the NLO susceptibilities increased as the atomic weights of halides increased.

4. Conclusions

The structural and optical properties of rhombohedral NLO crystals, $CsGe(Br_xCl_{1-x})_3$ ($x = 0$, 1/6, 2/6, 3/6, 4/6, 5/6 and 1), have been investigated experimentally to reveal the anion substitution effect. Based on the results, the linearly increasing x caused increase in lattice constant, second-order NLO susceptibility, but decay in bandgap values. Owing to the optical damage threshold and the transparent range of materials are related to the magnitude of the band gap, while the optical non-linearity is inversely proportional to the cubic power of the bandgap [8], we could modulate the nonlinear susceptibility coefficient, energy bandgap, laser damage threshold and transparency range of halides at the same time by anion substitution.

Acknowledgement

The authors are indebted to the financial support of the National Science Council of the Republic of China under the Grant, NSC 95-2112-M-009-042.

References

[1] D.M. Burland, Chem. Rev. 94 (1994) 1.
[2] J. Zyss, in: D.S. Chemla, J. Zyss (Eds.), Nonlinear Optical Properties of Organic Molecules and Crystals, Acadamic Press, Orlando, 1987.
[3] V.G. Dmitriev, G.G. Gurzadyan, D.N. Nikogosyan, Handbook of Nonlinear Optical Crystals, third ed., Springer-Verlag, Berlin, 1999.
[4] J. Zhang, N. Su, C. Yang, J. Qin, N. Ye, B. Wu, C. Chen, Chem. Proc. SPIE 3556 (1998) 1.
[5] M.D. Ewbank, F. Cunningham, R. Borwick, M.J. Rosker, P. Gunter, in: CLEO'97: Summaries of Papers Presented at the Conference on Lasers and Electro-Optics vol. 11, 1997, p. 462.
[6] L.C. Tang, C.S. Chang, J.Y. Huang, J. Phys.: Condens. Matter 12 (2000) 9129.
[7] Q. Gu, Q. Pan, X. Wu, W. Shi, C. Fang, J. Cryst. Growth 212 (2000) 605.
[8] Y.R. Shen, The Principles of Nonlinear Optics, John Wiley and Sons, 2002.
[9] Q. Gu, Q. Pan, W. Shi, X. Sun, C. Fang, Prog. Crys. Growth Characterizat. Mater. 40 (2000) 89.
[10] Q. Gu, C. Fang, W. Shi, X. Wu, Q. Pan, J. Crys. Growth 225 (2001) 501.
[11] A.N. Christensen, S.E. Rasmussen, Acta Chem. Scand. 19 (1965) 421.
[12] I.V. Tananaev, D.F. Dzhurinskii, Y.N. Mikhailov, Zh. Neorgan. Khim 9 (1964) 1570.
[13] W. Kraus, G. Nolze, J. Appl. Cryst. 29 (1996) 301.
[14] U. Schwarz, H. Hillebrecht, M. Kaupp, K. Syassen, H.G. von Schnering, G. Thiele, J. Solid State Chem. 118 (1995) 20.
[15] U. Schwarz, F. Wagner, K. Syassen, H. Hillebrecht, Phys. Rev. B 53 (1996) 12545.
[16] G. Thiele, H.W. Rotter, K.D. Schmidt, Z. Anorg. Allg. Chem. 545 (1987) 148.

[17] G. Thiele, H.W. Rotter, K.D. Schmidt, Z. Anorg. Allg. Chem. 559 (1988) 7.
[18] D.K. Seo, N. Gupta, M.H. Whangbo, H. Hillebrecht, G. Thiele, Inorg. Chem. 37 (1998) 407.
[19] J.I. Pankove, Optical Processes in Semiconductors, Prentice-Hall, Englewood Cliffs, NJ, 1971.
[20] W.K. Chen, C.M. Cheng, J.Y. Huang, W.F. Hsieh, T.Y. Tseng, J. Phys. Chem. Solids 61 (2000) 969.
[21] S.K. Kurtz, T.T. Perry, J. Appl. Phys. 39 (1968) 3798.
[22] J.P. Dougherty, S.K. Kurtz, J. Appl. Crystallogr. 9 (1976) 145.
[23] L.C. Tang, J.Y. Huang, C.S. Chang, M.H. Lee, L.Q. Liu, J. Phys.: Condens. Matter 17 (2005) 7275.
[24] V.M. Goldschmidt, Ber. Dtsch. Chem. Ges. 60 (1927) 1263.
[25] V.M. Goldschmidt, Fortschr. Min. 15 (1931) 73.
[26] R.D. Shannon, C.T. Prewitt, Acta Crystallogr. B 25 (1969) 925.
[27] R.D. Shannon, Acta Crystallogr. A 32 (1976) 751.